9456 *Biochemistry* **2009,** *48,* 9456–9465
DOI: 10.1021/bi900280u

BIOCHEMISTRY
including biophysical chemistry & molecular biology
Article

Functional Energetic Landscape in the Allosteric Regulation of Muscle Pyruvate Kinase. 2. Fluorescence Study[†]

Petr Herman*[,‡,§] and J. Ching Lee*[,§]

[‡]*Faculty of Mathematics and Physics, Institute of Physics, Charles University, Ke Karlovu 5, 121 16 Prague, Czech Republic, and* [§]*Department of Biochemistry and Molecular Biology, University of Texas Medical Branch, Galveston, Texas 77555-1055*

Received February 18, 2009; Revised Manuscript Received July 24, 2009

ABSTRACT: The energetic landscape of the allosteric regulatory mechanism of rabbit muscle pyruvate kinase (RMPK) was characterized by isothermal titration calorimetry (ITC). Four novel insights were uncovered. (1) ADP exhibits a dual property. Depending on the temperature, ADP can regulate RMPK activity by switching the enzyme to either the R or T state. (2) The assumption that ligand binding to RMPK is state-dependent is only correct for PEP but not Phe and ADP. (3) The effect of pH on the regulatory behavior of RMPK is partly due to the complex pattern of proton release or absorption linked to the multiple linked equilibria which govern the activity of the enzyme. (4) The R ↔ T equilibrium is accompanied by a significant ΔC_p, rendering RMPK most sensitive to temperature under physiological conditions. To rigorously test the validity of conclusions derived from the ITC data, in this study a fluorescence approach, albeit indirect, that tracks continuous structural perturbations was employed. Intrinsic Trp fluorescence of RMPK in the absence and presence of substrates phosphoenolpyruvate (PEP) and ADP, and the allosteric inhibitor Phe, was measured in the temperature range between 4 and 45 °C. For data analysis, the fluorescence data were complemented by ITC experiments to yield an extended data set allowing more complete characterization of the RMPK regulatory mechanism. Twenty-one thermodynamic parameters were derived to define the network of linked interactions involved in regulating the allosteric behavior of RMPK through global analysis of the ITC and fluorescent data sets. In this study, 27 independent curves with more than 1600 experimental points were globally analyzed. Consequently, the consensus results substantiate not only the conclusions derived from the ITC data but also structural information characterizing the transition between the active and inactive states of RMPK and the antagonism between ADP and Phe binding. The latter observation reveals a novel role for ADP in the allosteric regulation of RMPK.

In the previous article of this series (DOI: 10.1021/bi900279x), isothermal titration calorimetry (ITC) was employed to define the energy landscape of allosteric regulation of rabbit muscle pyruvate kinase (RMPK) (DOI: 10.1021/bi900279x). On the basis of a simple two-state model for the cooperative binding of ligands by macromolecules previously described by Monod and customized for the tertameric RMPK by Oberfelder et al. (*1*), four novel insights into the mechanism of allosteric regulation of RMPK were uncovered. (1) A temperature-dependent crossover of ADP affinity toward R and T states exists (more favorably to the R and T states at high and low temperatures, respectively). Thus, ADP not only serves as a substrate but also plays an important and intricate role in regulating RMPK activity. (2) The binding of Phe is negatively coupled to that of ADP in addition to the shifting of the R → T equilibrium. Thus, the assumption that ligand binding to RMPK is state-dependent is only correct for PEP but not for Phe and ADP. (3) The release or absorption of protons linked to the various equilibria is specific to the particular reaction. As a consequence, pH will exert a complex effect on these linked equilibria with the net effect being manifested in the regulatory behavior of RMPK. (4) The R ↔ T equilibrium is accompanied by a significant ΔC_p enabling the change of state of RMPK to be particularly sensitive under physiological conditions. While the approach of ITC is versatile and powerful, it is an indirect measurement that does not identify the specific interaction among the many linked reactions. Reactions with significant heat change may dominate the signal and obscure others. Thus, we wish to acquire data that are complementary to the ITC data. The complementarity should provide a signal from structural changes. In this study, a fluorescence approach, albeit indirect, that tracks continuous structural perturbations was employed.

The choice of fluorescence is based on the fact that execution of biological function by proteins depends highly on an internal mobility encoded by their structures and sequences. These movements are inherent to the structure and to the interactions within the molecule (*5*). In fact, proteins even in their native states assume different conformations differing in terms of structural details (*6*, *7*). Because of the high sensitivity of indole emission to local interactions and changes in the microenvironment induced by conformational changes, either local or involving the entire macromolecule, tryptophan residues are excellent intrinsic probes for fluorescent monitoring of protein structural transitions in

[†]Supported by National Institutes of Health Grant GM 77551 and the Robert A. Welch Foundation (J.C.L.) and Grant MSM 0021620835 of the Ministry of Education, Youth and Sports of the Czech Republic (P.H.).

*To whom correspondence should be addressed. J.C.L.: telephone, (409) 772-2281; fax, (409) 772-4298; e-mail, jclee@utmb.edu. P.H.: telephone, +420-221911461; fax, +420-224922797; e-mail, herman@karlov.mff.cuni.cz.

 Published on Web 08/31/2009

FIGURE 1: Structure of RMPK. Color and domain assignments are as follows: blue for B (residues 116−218), red for A (residues 12−115 and 219−387), yellow for C (residues 388−530), green sphere for the active site, cyan spheres for tryptophan residue 157 in domain B and tryptophan residues 481 and 514 in domain C [Protein Data Bank (PDB) entry 1F3W].

solution (*8*, *9*). Thus, fluorescence of tryptophan residues is employed as the probe to track ligand binding and structural changes.

Analysis of X-ray data revealed that each RMPK subunit is composed of three major domains (*10*), as shown in Figure 1. The B domain is exposed to the solvent and is attached to the central A domain by a flexible hinge region. Domains A and B form a cleft adjacent to the active site. Previous studies indicated that binding of metabolites induces changes in the hydrodynamic properties of RMPK (*1*, *11*−*13*). In particular, binding of PEP and metal ions required for activity causes the enzyme to assume a compact symmetric conformation (the R state), whereas the allosteric inhibitor Phe converts RMPK to the inactive form with a significantly expended structure (the T state). Since the secondary structure of the enzyme was shown to remain unaltered (*14*), significant domain movement must take place during the conformational transitions from the active to the inactive state. Because each RMPK subunit contains three Trp residues that can serve as intrinsic probes, these transitions can be followed by Trp fluorescence. Two Trp residues are located in the C domain, and Trp157 is located in the movable B domain near the binding site (*15*). This location is very favorable for fluorescent monitoring of ligand binding.

In this study, the environmental sensitivity of Trp fluorescence was employed for spectroscopic monitoring of the R ↔ T equilibrium shifts induced by PEP, ADP, and Phe binding. Fluorescence data sets were simultaneously analyzed with the ITC data from the preceding paper (DOI: 10.1021/bi900279x). This complex approach allowed an "over"-determination of the model with multiple overlapping signal and extraction of thermodynamic parameters that could not be accessed by analysis of single curves or the ITC data only.

MATERIALS AND METHODS

Materials. Samples preparations and material were identical to procedures described in detail in the preceding paper (DOI: 10.1021/bi900279x).

Fluorescence. Fluorescence experiments were performed on the SLM 8000 spectrofluorometer in TKM buffer (at pH 7.5 it contained 50 mM Trizma base, 72 mM KCl, and 7.2 mM $MgSO_4$) at a protein concentration of 0.1 mg/mL. The temperature of the sample was measured in a cuvette with a thermocouple (BAT-12) with an accuracy of ±0.15 °C.

Isothermal Fluorescent Titration (*IFT*). Ligands were added to the sample by an automatic buret (ABU80, Radiometer Copenhagen) remotely controlled by TTL signals from the fluorometer. Samples were gently mixed with a magnetic stirrer during the titration. To avoid inner filter effects caused by an addition of ligands and by protein dilution as well as an excitation of tyrosines, the excitation wavelength was set to 300 nm (1 nm slit width). The fluorescence of RMPK was collected at 350 nm, where the contribution of Raman scattering generated by the excitation light in the aqueous solvent was negligible. All titrations were repeated with buffer substituted for the sample, and the background signal was collected. Raw fluorescence data were corrected for a dilution of protein and for a small background emission of buffer and ligands. Then the IFT curves were normalized by the fluorescence intensity of the unliganded RMPK. The normalization factor was determined at the beginning of every titration. A dedicated computer program was developed for these automatic fluorescence titrations.

Fluorescence Temperature Scan (*FTS*). Four samples were prepared and placed in a four-cell temperature-controlled cuvette holder in the spectrofluorometer. In particular, the first cuvette contained unliganded RMPK; the second cuvette contained the same RMPK concentration with a saturating concentration of a ligand, and the third and fourth cuvettes contained buffer and buffer with the ligand, respectively. Then the corrected intensity ratio $\{I_{lig}/I_0 = [I_{(pk+lig)} - I_{(buf+lig)}]/(I_{PK} - I_{buf})\}$ was automatically measured as a function of temperature. The temperature was slowly increased with a programmable water bath (Neslab, RTE-110) at a rate of 0.2 °C/min. This rate of increase was sufficiently slow to guarantee that intensity readings from all four cuvettes were taken at the same temperature. The temperature of the sample was measured directly in the cuvette at the very moment of data acquisition using a thermocouple thermometer (Physitemp, BAT-12) connected to the data acquisition board (DAP 1200e/6). Temperature readings and data logging were synchronized by TTL signals with the spectrofluorometer. A dedicated computer program was developed for instrumental control. The tryptophan emission was isolated by a combination of a UG1 absorption filter and a long-pass filter with a cutoff wavelength of 345 nm. To eliminate the temperature-induced pH shift of the TKM buffer, samples were changed every 5 °C and the buffer with the pH corrected for the temperature change was used. Therefore, the sample pH never differed more than ±0.06 pH unit from the preset value of 7.50. The reversibility of the observed fluorescence changes was monitored by a repetition of the heating−cooling cycle with the same sample. Data from repeated measurements overlapped with the original ones. The complete titration curves were constructed by overlapping the data from adjacent temperature intervals.

Global Fitting. Global fitting (*16*) is a powerful method for discerning between models and recovery of model parameters. It has been described in detail previously (*16*, *17*). The method is based on an ordinary nonlinear least-squares fitting (*18*), and it allows for simultaneous analysis of multiple data sets acquired under different conditions and with different techniques. During the global fitting, the overall sum of weighted squared deviations of

calculated values from the measured data (χ^2) is minimized to yield model parameters that are consistent with all data sets. An in-house program utilizing the Marquardt−Levenberg minimization procedure (*19*) was employed to simultaneously analyze both the fluorescence and the previously published ITC data (DOI: 10.1021/bi900279x). The model described in the preceding paper (DOI: 10.1021/bi900279x) and extended in this paper encompassed all the experimental data by a complex linkage of thermodynamic parameters between different data sets. As a consequence, many model parameters were inherently common for several different data sets. Such an overdetermination helped validate the model and recover the model parameters with a resolving power unequaled by a conventional data analysis (*20*−*26*).

Model Description. Our model is based on a two-state model for cooperative binding of ligands to macromolecules that has been published by Monod et al. (*27*) and adapted by Oberfelder et al. (*1*) for the tetrameric RMPK. Description and application of this model for analysis of calorimetric RMPK data can be found in the preceding paper (DOI: 10.1021/bi900279x). Briefly, experimental data suggest (*1*−*3*, *11*) that unliganded RMPK assumes two major conformations that are in equilibrium, R ↔ T. Enzyme in the R state exhibits high activity; T is an inactive state. The equilibrium constant between the two unliganded states is

$$L_0 = [\mathrm{T}_0]/[\mathrm{R}_0] \tag{1}$$

and a temperature dependence of L_0 is given by the equation

$$-RT \times \ln(L_0) = \Delta H_{\mathrm{R}\leftrightarrow\mathrm{T}} - T\Delta S_{\mathrm{R}\leftrightarrow\mathrm{T}} \tag{2}$$

where $\Delta H_{\mathrm{R}\rightarrow\mathrm{T}}$ and $\Delta S_{\mathrm{R}\rightarrow\mathrm{T}}$ are the enthalpy and entropy change, respectively, associated with the R → T transition. Calorimetric data have shown that an isobaric heat capacity change is associated with the transition; therefore

$$\Delta H_{\mathrm{R}\leftrightarrow\mathrm{T}} = \Delta H_{0,\,\mathrm{R}\leftrightarrow\mathrm{T}} + \Delta C_{p,\,\mathrm{R}\leftrightarrow\mathrm{T}}(T - T_0) \tag{3}$$

and

$$\Delta S_{\mathrm{R}\leftrightarrow\mathrm{T}} = \Delta S_{0,\,\mathrm{R}\leftrightarrow\mathrm{T}} + \Delta C_{p,\,\mathrm{R}\leftrightarrow\mathrm{T}}(T - T_0) \tag{4}$$

In the presence of a single ligand, the ligand binds to both states and the reaction scheme changes to

$$\begin{array}{ccccccc} & & & & L_0 & & \\ \mathit{Ligand} & + & \mathit{R} & \leftrightarrows & \mathit{T} & + & \mathit{Ligand} \\ & & \updownarrow & & \updownarrow & & \\ & & \mathit{R(liganded)} & \leftrightarrows & \mathit{T(liganded)} & & \end{array}$$

This is a multiple-equilibrium system in which dissociation constants $K_{\mathrm{lig}}^{\mathrm{state}}$ of the ligand to the R and T states are temperature-dependent:

$$RT \times \ln(K_{\mathrm{lig}}^{\mathrm{state}}) = \Delta H_{\mathrm{lig}}^{\mathrm{state}} - T\Delta S_{\mathrm{lig}}^{\mathrm{state}} \tag{5}$$

To quantitatively describe fluorescence changes induced by separate or simultaneous binding of one substrate (ADP or PEP) and the inhibitor (Phe) to RMPK, we assumed that each multiply liganded R state (R_{ij}) and T state (T_{ij}) has a unique fluorescence quantum yield characterized by fluorescent coefficients a_{ij} and b_{ij}, respectively. The subscript *i* and *j* denote the number of substrate and inhibitor molecules, respectively, bound to the RMPK tetramer. Since each RMPK subunit has a unique binding site for each substrate and for the inhibitor as well, both subscripts assume values from 0 to 4. For example, $[\mathrm{R}_{23}]$ is the concentration of the R state with two molecules of one of the substrates and three molecules of inhibitor bound; $[\mathrm{T}_{00}]$ is the concentration of an unliganded RMPK tetramer in the T state.

The ligation-dependent part of a_{ij} and b_{ij} is a minor perturbation on the level of a subunit that contributes to a small extent in addition to the major, ligation-independent, change in the fluorescent coefficients caused by the concerted R ↔ T transition. The binding-dependent modulation of the emission quantum yield may have multiple origins. Since the intramolecular quenching does not necessarily need an actual collision of the groups, the quantum yield can be influenced by long-range through-space interactions, e.g., by a binding-induced change in the local electrostatic field (*41*). Intensity variations can be also coupled to changes in the subunit internal dynamics that can change upon ligand binding (*42*).

The measured emission intensity can be calculated as a simple sum of intensities over all possible ligation states:

$$I = C\frac{\sum_{i,j=0}^{4}(a_{ij}[\mathrm{R}_{ij}] + b_{ij}[\mathrm{T}_{ij}])}{\sum_{i,j=0}^{4}([\mathrm{R}_{ij}] + [\mathrm{T}_{ij}])} \tag{6}$$

where *C* is a proportionality constant, including quantum yield and instrumental parameters. Intensity I_0 of the unliganded state is therefore

$$I_0 = C\frac{a_{00} + L_0 b_{00}}{1 + L_0} \tag{7}$$

where L_0 ($= [\mathrm{T}_{00}]/[\mathrm{R}_{00}]$) is the equilibrium constant for the R ↔ T equilibrium. $[\mathrm{R}_{ij}]$ and $[\mathrm{T}_{ij}]$ can be expressed as (*28*)

$$[\mathrm{R}_{ij}] = R_{00}\binom{4}{i}\binom{4}{j}\left(\frac{[\mathrm{Sub}]}{K_{\mathrm{Sub}}^{\mathrm{R}}}\right)^i\left(\frac{[\mathrm{Inh}]}{K_{\mathrm{Inh}}^{\mathrm{R}}}\right)^j \tag{8}$$

$$[\mathrm{T}_{ij}] = T_{00}\binom{4}{i}\binom{4}{j}\left(\frac{[\mathrm{Sub}]}{k_{\mathrm{Sub}}^{\mathrm{T}}}\right)^i\left(\frac{[\mathrm{Inh}]}{k_{\mathrm{Inh}}^{\mathrm{T}}}\right)^j \tag{9}$$

where [Sub] and [Inh] are concentrations of a chosen substrate and inhibitor, respectively, and $K_{\mathrm{Sub}}^{\mathrm{state}}$ and $K_{\mathrm{Inh}}^{\mathrm{state}}$ are dissociation constants from the R and T states of RMPK, respectively. After substitution of eqs 8 9 into eq 6 and normalization of the result by I_0 (eq 7), then

$$\frac{I}{I_0} = \frac{1 + L_0}{1 + \tilde{b}_{00}L_0}\frac{\sum_{i,j=0}^{4}\binom{4}{i}\binom{4}{j}[\mathrm{Sub}]^i[\mathrm{Inh}]^j[\tilde{a}_{ij}(K_{\mathrm{Sub}}^{\mathrm{R}})^{-i}(K_{\mathrm{Inh}}^{\mathrm{R}})^{-j} + \tilde{b}_{ij}L_0(K_{\mathrm{Sub}}^{\mathrm{T}})^{-i}(K_{\mathrm{Inh}}^{\mathrm{T}})^{-j}]}{\sum_{i,j=0}^{4}\binom{4}{i}\binom{4}{j}[\mathrm{Sub}]^i[\mathrm{Inh}]^j[(K_{\mathrm{Sub}}^{\mathrm{R}})^{-i}(K_{\mathrm{Inh}}^{\mathrm{R}})^{-j} + L_0(K_{\mathrm{Sub}}^{\mathrm{T}})^{-i}(K_{\mathrm{Inh}}^{\mathrm{T}})^{-j}]} \tag{10}$$

Equation 10 is temperature-dependent because of the temperature dependence of L_0 and all dissociation constants (eqs 2−5). Normalized fluorescence coefficients ($\tilde{a}_{ij} = a_{ij}/a_{00}$, and $\tilde{b}_{ij} = b_{ij}/a_{00}$) characterize relative fluorescence changes upon binding of a ligand. The reference state is the unliganded R state. For modeling of the $\tilde{a}_{ij}$ and $\tilde{b}_{ij}$ coefficients, we assumed that each binding event of the particular ligand causes the same fluorescence change. This seems to be a reasonable first-order approximation for homotetrameric RMPK where the binding-induced fluorescence change can be envisioned as a direct perturbation of the Trp microenvironment by the ligand on the level of the subunit. Then $\tilde{a}_{ij}$ and $\tilde{b}_{ij}$ can be calculated as

$$\tilde{a}_{ij} = 1 + i\xi^{R}_{Sub} + j\xi^{R}_{Inh} \quad \tilde{b}_{ij} = \tilde{b}_{00} + i\xi^{T}_{Sub} + j\xi^{T}_{Inh} \quad (11)$$

The term $\tilde{b}_{00}$ represents the relative fluorescence intensity of the unliganded T state relative to the intensity of the unliganded R state and reflects a structural difference between the two states. ξ^{state}_{Sub} and ξ^{state}_{Inh} are terms for fluorescence increments caused by a single binding event on the level of one RMPK subunit. Depending on the nature of perturbation, these increments can generally be either negative or positive. Equation 10 can be used to calculate I/I_0 for any concentration of a single substrate (ADP or PEP) in the presence of any fixed concentration of inhibitor.

Temperature dependence of the fluorescence intensity $^{sat}I_{lig}$ for RMPK saturated by a single ligand (this can be either substrate or inhibitor), relative to the fluorescence intensity of unliganded enzyme I_0, can be derived from eq 10 using eq 11. For a high concentration of ligand (when RMPK is fully saturated), we obtain

$$\frac{^{sat}I_{lig}}{I_0} = \lim_{[lig]\to\infty}\left(\frac{I}{I_0}\right) = \frac{1+L_0}{1+\tilde{b}_{00}L_0}\,\frac{1+4\xi^{R}_{lig}+L_0(K^{R}_{lig}/K^{T}_{lig})^4(\tilde{b}_{00}+4\xi^{T}_{lig})}{1+L_0(K^{R}_{lig}/K^{T}_{lig})^4} \quad (12)$$

At a saturating PEP concentration and between 5 and 45 °C, the RMPK molecule was shown to be fully in the R state as a consequence of the preferential binding of PEP to the active state (DOI: 10.1021/bi900279x). Then the term $L_0(K^{R}_{PEP}/K^{T}_{PEP})^4 \ll 1$ may be neglected, and eq 12 is reduced to

$$\frac{^{sat}I_{PEP}}{I_0} = \frac{(1+L_0)(1+4\xi^{R}_{PEP})}{1+\tilde{b}_{00}L_0} \quad (13)$$

Similarly, at a saturating Phe concentration, the R ↔ T equilibrium was in favor of the T state by preferential binding of Phe to this state. As a consequence, $L_0(K^{R}_{Phe}/K^{T}_{Phe})^4 \gg 1$ and eq 12 reduces to

$$\frac{^{sat}I_{Phe}}{I_0} = \frac{(1+L_0)(\tilde{b}_{00}+4\xi^{T}_{Phe})}{1+\tilde{b}_{00}L_0} \quad (14)$$

When eq 14 is divided by eq 13, we obtain a measurable quantity:

$$\frac{^{sat}I_{Phe}}{^{sat}I_{PEP}} = \frac{\tilde{b}_{00}+4\xi^{T}_{Phe}}{1+4\xi^{R}_{PEP}} \quad (15)$$

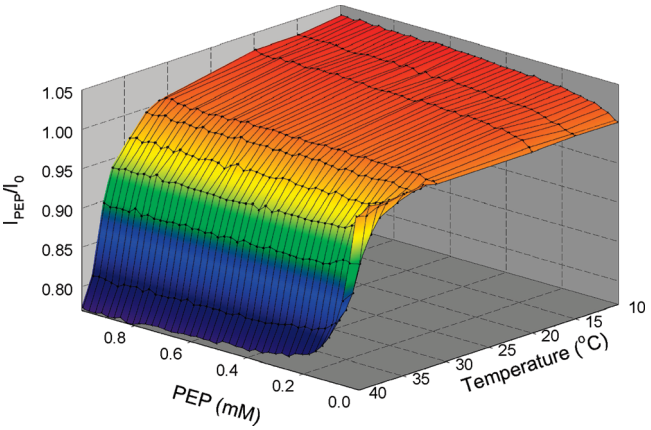

FIGURE 2: Normalized fluorescence intensity of RMPK as a function of temperature and PEP concentration.

Importantly, eq 15 shows that the $^{sat}I_{Phe}/^{sat}I_{PEP}$ ratio is a function of the fluorescence coefficients only, and as a consequence, information about the temperature dependence of these coefficients can be extracted from the experimentally measured $^{sat}I_{Phe}/^{sat}I_{PEP}$.

RESULTS

Ligand Binding Isotherms: Isothermal Fluorescence Titration (*IFT*). To gain further insight into the allosteric regulation of RMPK, we performed equilibrium titrations of RMPK by its ligands to define ligand binding isotherms. All titrations were executed in the temperature range between 4 and 45 °C. At each temperature, the titration curve was normalized by the fluorescence intensity of the unliganded RMPK, I_0. The normalization allowed elimination of a temperature dependence of the fluorescence intensity of the unliganded RMPK. Direct comparison of the shape of these binding curves was then possible.

(*i*) *PEP Binding*. Titration curves of RMPK with PEP at different temperatures are shown in Figure 2. Visual inspection of the figure indicates that the fluorescence quantum yield of the R state is lower than that of the T state, which is evident in a gradual increase in I_{PEP}/I_0 at low temperatures and a sharp decrease above 30 °C where the fraction of the unliganded T state is known to significantly increase (DOI: 10.1021/bi900279x and DOI: 10.1021/bi900281s) (*3*). Because of the preferential affinity of PEP for the R state, the presence of PEP shifts the enzyme population toward the R state, resulting in a decrease in fluorescence intensity. Because the fraction of the T state in the unliganded RMPK increases with an increase in temperature, a larger PEP-induced fluorescence decrease was observed at elevated temperatures. The small fluorescence increase recorded at low temperatures, where RMPK is fully in the R state, is evidence of an additional binding-induced perturbation of the fluorescence quantum yield that is superimposed on the more significant fluorescence change caused by the R ↔ T equilibrium shift. Because there are no indications of cooperativity in this region of the small fluorescence increase, the change can be assigned to a direct perturbation of the Trp microenvironment by PEP binding at the level of the RMPK subunit.

(*ii*) *Phe Binding*. Fluorescence changes induced by the binding of the inhibitor Phe at different temperatures are shown in Figure 3. At all temperatures, an increasing Phe concentration induces a gradual increase in the I_{Phe}/I_0 ratio. The increase reaches a plateau at saturation. Figure 3 shows that the plateau

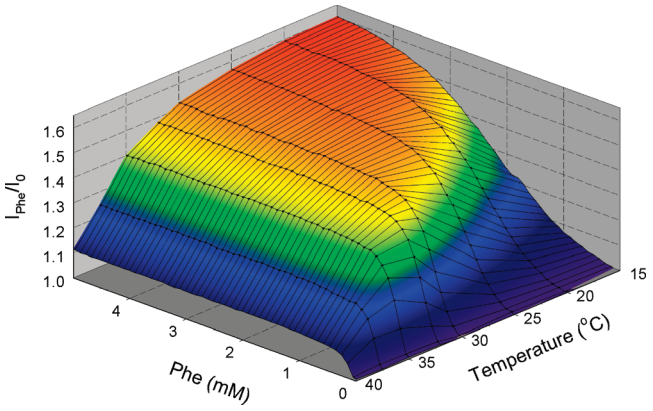

FIGURE 3: Normalized fluorescence intensity of the RMPK as a function of temperature and Phe concentration.

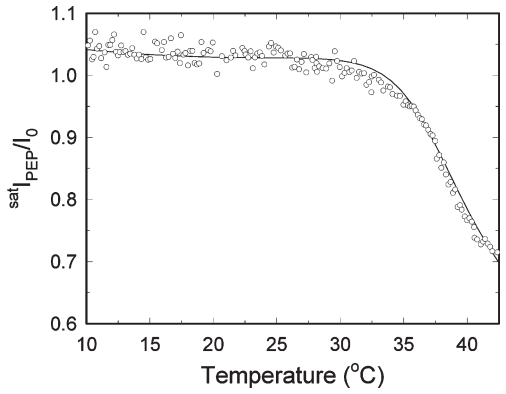

FIGURE 4: Fluorescence intensity of RMPK saturated with 2 mM PEP relative to the fluorescence intensity of the unliganded enzyme. The solid line represents the best overall global fit.

intensity, as well as the sigmoidicity of the curve, significantly decreases with an increase in temperature. These data confirm that the fluorescence quantum yield of the R state is lower than that of the T state. The preferential affinity of Phe for the T state results in a shift of the RMPK population toward the T state when the Phe concentration increases. The increase is therefore accompanied by an increasing fluorescence intensity. This is evident especially at low temperatures when RMPK is fully in the "low-emission" R state. A temperature elevation shifts the R ↔ T equilibrium toward the T state. As a consequence, a smaller fraction of RMPK can be converted to the T state by Phe binding and the magnitude of the intensity increase becomes less pronounced. The sigmoidal shape of the IFT curves is in good agreement with the proposed concerted nature of the R ↔ T transition. Binding of a single Phe molecule to the tetrameric RMPK causes a concerted transition of all enzyme subunits from the active to the inactive state which has a significantly higher binding affinity for Phe. Binding of Phe to these high-affinity binding sites therefore becomes apparent after a single Phe binds to the unliganded RMPK in the R state. As a consequence, a sigmoidal binding curve is observed. The observed fluorescence changes are qualitatively in good agreement with the two-state concerted model proposed for the allosteric regulation of RMPK (DOI: 10.1021/bi900279x) (*1*−*3*, *11*).

Structural Perturbation: Fluorescence Temperature Scan (*FTS*). (*i*) *Effect of PEP*. Figure 4 shows the detailed temperature dependence of the $^{sat}I_{PEP}/I_0$ ratio at a saturating PEP concentration (2 mM). The profile qualitatively resembles

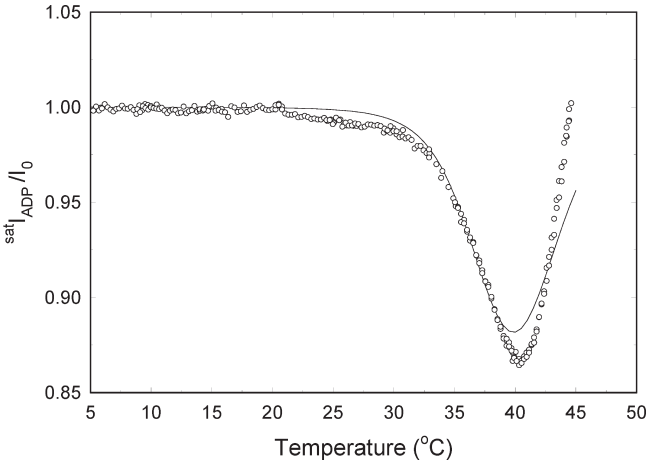

FIGURE 5: Temperature dependence of the RMPK fluorescence intensity in the presence of 10 mM ADP normalized by the fluorescence intensity of the unliganded enzyme. The solid line is a dependence predicted by the model.

the shape of the calorimetric data for PEP binding, shown in the preceding paper (DOI: 10.1021/bi900279x).

(*ii*) *Effect of ADP*. Similarity between the ITC and the fluorescence data is observed also for the temperature scan in the presence of 10 mM ADP, as shown in Figure 5. A decrease in the $^{sat}I_{ADP}/I_0$ ratio in Figure 5 indicates activation of RMPK by ADP at temperatures between 30 and 40 °C. Such an observation is caused by shifting of the R ↔ T equilibrium to the R state which is characterized by a low quantum yield. The subsequent fluorescence increase above 40 °C indicates that the ADP-induced activation is outweighed by a shift of the R ↔ T equilibrium to the T state. The observed increase is not a result of an irreversible thermal denaturation because the observed fluorescence changes were always reversible as indicated by a return to the initial signal with a reversal of the temperature. Indeed, the titration curves from the calorimetric and fluorescence experiments should resemble each other because these experiments are the same with the only difference being the method of detection.

(*iii*) *Effect of Phe and ADP*. The published ITC data (DOI: 10.1021/bi900279x) as well as the fluorescence experiments shown in this study prove that ADP exhibits temperature-dependent differential affinity for the R and T states; therefore, its binding influences the R ↔ T equilibrium. An antagonism between Phe and ADP was detected in the published ITC data (DOI: 10.1021/bi900279x). However, it is important to secure independent data to test the validity of the conclusions derived from the ITC data. Results of our fluorescence measurements can provide the necessary information. Since the fluorescence quantum yield of the R state is lower than that of the T state, the shift of the R ↔ T equilibrium can be monitored by fluorescence intensity. If the enzyme in the presence of ADP and a saturating concentration of Phe was in the T state at all temperatures, then the $^{sat}I_{ADP,Phe}/^{sat}I_{Phe}$ ratio should be essentially independent of temperature and ADP concentration. Figure 6 shows a temperature dependence of the $^{sat}I_{ADP,Phe}/^{sat}I_{Phe}$ ratio at a saturating Phe concentration of 12 mM and three different concentrations of ADP. At a low ADP concentration (1 mM), the $^{sat}I_{ADP,Phe}/^{sat}I_{Phe}$ ratio is temperature-independent, indicating that 1 mM ADP does not exert any significant effect on the redistribution of the R and T states. At 2 mM ADP, however, the ratio starts out at a lower value at low temperatures. At 10 mM ADP, a significant

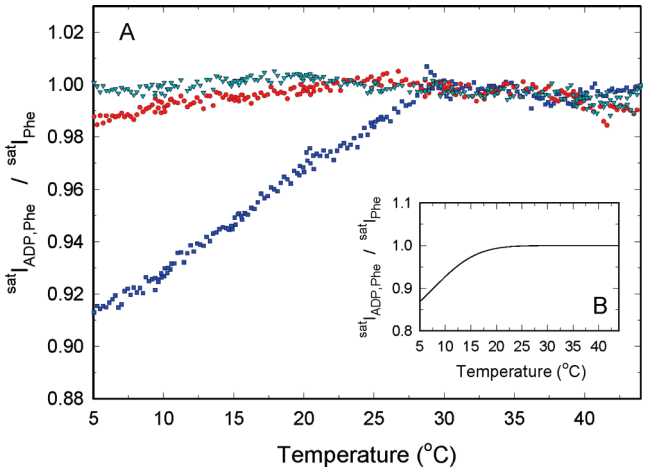

FIGURE 6: Fluorescence temperature scans. (A) Fluorescence intensity of RMPK saturated with 12 mM Phe in the presence of 1 (green), 2 (red), and 10 mM ADP (blue). The intensities are normalized by the fluorescence intensity of RMPK saturated with 12 mM Phe. (B) Predicted temperature dependence of $^{sat}I_{ADP,Phe}/^{sat}I_{Phe}$ calculated from model parameters obtained by global fitting.

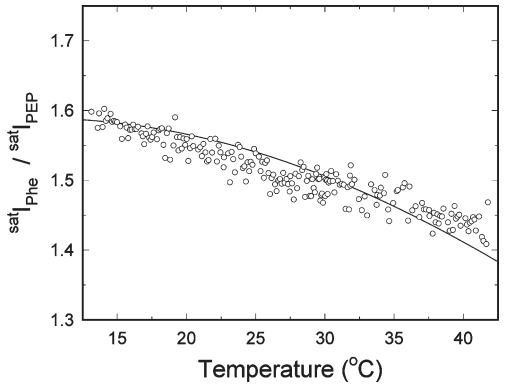

FIGURE 7: Fluorescence intensity of RMPK in the presence of 2 mM PEP relative to the fluorescence intensity of PK saturated with 12 mM Phe. The solid line represents the best overall global fit.

decrease was observed. Data from Figure 6 suggest that at low temperatures the ADP binding overcomes the inhibiting effect of Phe by shifting a fraction of RMPK to the R state. This is a consequence of both the differential affinity of ADP and an altered differential affinity of Phe for the R and T states.

Parameterization of the Model. In the fluorescence model described in Materials and Methods, we assumed that each multiply liganded R state (R_{ij}) and T state (T_{ij}) has a unique fluorescence quantum yield and, as a consequence, the I/I_0 ratio can be characterized by normalized fluorescent coefficients $\tilde{a}_{ij}$ and $\tilde{b}_{ij}$, respectively (see eqs 10 and 11). Indices i and j denote the number of substrate and inhibitor molecules, respectively, bound to the RMPK tetramer. The FTS curve shown in Figure 7 provides the data that indicate that these coefficients are temperature-dependent. If the coefficients $\tilde{a}_{ij}$ and $\tilde{b}_{ij}$ were temperature-independent, the measured $^{sat}I_{Phe}/^{sat}I_{PEP}$ ratio should be constant as suggested by eq 15. Instead, a decrease in this ratio with an increase in temperature was observed. The temperature dependence of the $^{sat}I_{Phe}/^{sat}I_{PEP}$ ratio implies that parameters $\tilde{b}_{00}$, ξ^{R}_{PEP}, and ξ^{T}_{Phe} from eq 15, or some of them, are temperature-dependent. This conclusion is not surprising because proteins are dynamic structures in which the extent of internal mobility depends on temperature. Therefore, ligand-induced conformational changes in the RMPK structure perturbing the fluorescence response can be temperature-dependent. Not having a priori information about the functional form of this dependence, we incorporated it into the model as a quadratic function of temperature:

$$\tilde{b}_{00} = {}^{0}\tilde{b}_{00} + {}^{1}\tilde{b}_{00}T + {}^{2}\tilde{b}_{00}T^2 \quad (16)$$

$$\xi^{state}_{ligand} = {}^{0}\xi^{state}_{ligand} + {}^{1}\xi^{state}_{ligand}T + {}^{2}\xi^{state}_{ligand}T^2 \quad (17)$$

To keep the model as simple as possible, the coefficients ${}^{i}\xi^{T}_{PEP}$ and ${}^{i}\xi^{R}_{Phe}$ (i = 0, 1, or 2) associated with the "weak binding" of PEP to the T state and Phe to the R state were set to zero at all temperatures since these binding constants are small.

Global Fitting of Calorimetric and Fluorescence Data Sets. Quality of the Fit. Having the model properly parametrized, we performed a global fit of all curves from Figures 2–4 and 7. To overdetermine the model as much as possible (i.e., the same parameter was experimentally defined by multiple techniques under a variety of conditions), the full set of ITC curves from the preceding paper (DOI: 10.1021/bi900279x) was included in the analysis. Such combination allows for better verification of the model and for more accurate recovery of model parameters. The target parameters in the analysis were enthalpies and entropies of the characterized equilibrium

Table 1: Parameters Obtained from Global Fitting of the IFT, FTS, and ITC[a] Data Sets

reaction	parameter	value	unit[b]
R ↔ T	$\Delta S_{0,R\rightarrow T}$	154 (3)[d,f]	cal mol^{-1} K^{-1}[c]
	$\Delta H_{0,R\rightarrow T}$	49 (4)[d]	kcal mol^{-1}[c]
	$\Delta C_{p,R\rightarrow T}$	2.2 (0.2)[d]	kcal mol^{-1} K^{-1}[c]
	$\Delta n_{R\rightarrow T}$	0.7 (0.1)[e]	mol^{-1}[c]
Phe binding	ΔS^{R}_{Phe}	2.7 (0.9)	cal mol^{-1} K^{-1}
	ΔH^{R}_{Phe}	−1.4 (0.4)	kcal mol^{-1}
	ΔS^{T}_{Phe}	18.2 (0.2)	cal mol^{-1} K^{-1}
	ΔH^{T}_{Phe}	0.65 (0.20)	kcal mol^{-1}
	Δn^{T}_{Phe}	−1.0 (0.1)	mol^{-1}
PEP binding	$\Delta S^{R}_{0,PEP}$	11.2 (0.2)	cal mol^{-1} K^{-1}
	$\Delta H^{R}_{0,PEP}$	−2.1 (0.3)	kcal mol^{-1}
	Δn^{R}_{PEP}	0.18 (0.03)	mol^{-1}
ADP binding	ΔS^{R}_{ADP}	−20 (2)	cal mol^{-1} K^{-1}
	ΔH^{R}_{ADP}	−10.5 (1.0)	kcal mol^{-1}
	Δn^{R}_{ADP}	0.75 (0.02)	mol^{-1}
	ΔS^{T}_{ADP}	−28 (2)	cal mol^{-1} K^{-1}
	ΔH^{T}_{ADP}	−12.8 (1.0)	kcal mol^{-1}
	Δn^{T}_{ADP}	0.98 (0.02)	mol^{-1}
ADP−Phe coupling	$\Delta\Delta S^{T}_{ADP,PHe}$	−4.9 (0.5)	cal mol^{-1} K^{-1}
	$\Delta\Delta H^{T}_{ADP,PHe}$	−0.54 (0.30)	kcal mol^{-1}
	$\Delta n^{R}_{ADP,Phe}$	−0.9 (0.5)	mol^{-1}
fluorescence parameters	${}^{0}\tilde{b}_{00}$	227 (3)	
	${}^{1}\tilde{b}_{00}$	−1.48 (0.01)	
	${}^{2}\tilde{b}_{00}$	2.43 (2.00) × 10^{-3}	
	${}^{0}\xi^{R}_{PEP}$	1.80 (0.02)	
	${}^{1}\xi^{R}_{PEP}$	−1.22 (0.01) × 10^{-2}	
	${}^{2}\xi^{R}_{PEP}$	2.06 (3.00) × 10^{-5}	
	${}^{0}\xi^{T}_{Phe}$	−57.3 (0.3)	
	${}^{1}\xi^{T}_{Phe}$	3.78 (0.01) × 10^{-1}	
	${}^{2}\xi^{T}_{Phe}$	−6.22 (14.00) × 10^{-4}	

[a] Isothermal titration calorimetry data published in the preceding paper (DOI: 10.1021/bi900279x) were used together with the fluorescence data for global fitting. [b] Per mole of ligand. [c] Per molw of tetramer. [d] For T_0 = 20 °C. T_0 was a fixed parameter. [e] Amount of protons absorbed (positive value) or released (negative value). Buffer ionization heats are 11.3 and 6.8 kcal/mol for TKM and BTKM, respectively (*40*). [f] Standard deviations are given in parentheses.

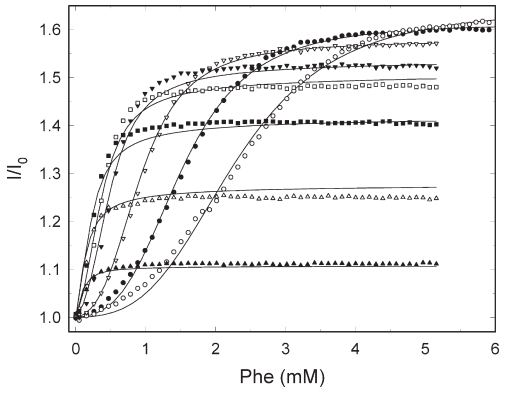

FIGURE 8: Fluorescence titration curves of RMPK titrated with Phe at 15 (○), 20 (●), 25 (▽), 30 (▼), 32 (□), 35 (■), 37.5 (△), and 40 °C (▲). Solid lines represent the best overall global fit.

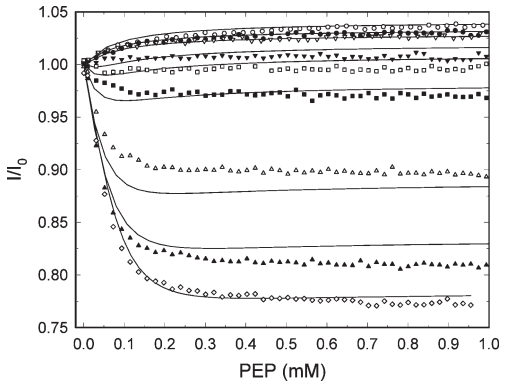

FIGURE 9: Fluorescence titration curves of RMPK titrated with PEP at 10 (○), 15 (●), 20 (▽), 31 (▼), 32.5 (□), 34.5 (■), 37.5 (△), 39 (▲), and 40 °C (◇).

reactions, linked protonations, and fluorescence coefficients. Results are summarized in Table 1. Where applicable, values from the calorimetry paper were used as an initial guess (DOI: 10.1021/bi900279x).

The best global fit is presented in Figures 4, 6, 8, and 9 by solid lines.[1] The reproducibility of the fluorescence measurements within weeks with the same batch of protein was ~2%. The reproducibility of the experiments within months and different batches of RMPK was ~6−10%. Examination of the quality of the fit reveals good agreement of the model with the measured data taking into account the fact that 27 curves were simultaneously fitted. Some systematic deviations of the fit from the PEP titration data, as shown in Figure 9, are on the order of the experimental reproducibility. The fit in Figure 9 cannot simply be corrected by additional parameters, e.g., by incorporation of a non-zero heat capacity change for PEP binding, $\Delta C_{p,\mathrm{PEP}}$. Addition of $\Delta C_{p,\mathrm{PEP}}$ as a fitting parameter yielded a rather small value of −0.03 kcal mol^{-1} deg^{-1} without a noticeable improvement in the fit. The cause of such systematic deviations could be a more complex dependence of the fluorescence intensity on temperature and ligation state. A resolution of this issue will depend on additional data from another approach.

Seventeen of the 21 thermodynamic parameters obtained by global fitting of both the ITC and the fluorescence data are in good agreement with the parameters obtained by global fitting of calorimetry data alone (DOI: 10.1021/bi900279x). Even for the four remaining thermodynamic parameters, namely, $\Delta S^{\mathrm{R}}_{\mathrm{Phe}}$, $\Delta H^{\mathrm{R}}_{\mathrm{Phe}}$, $\Delta\Delta S^{\mathrm{T}}_{\mathrm{ADP,Phe}}$, and $\Delta\Delta S^{\mathrm{T}}_{\mathrm{ADP,Phe}}$, the differences are within the uncertainties estimated for the ITC data alone.

Parameters Derived from the Global Fit. (*i*) *R → T Transition*. Table 1 shows that an unfavorable enthalpy change of ~50 kcal/mol of enzyme is associated with the temperature-dependent R → T transition. The state transition is therefore driven by a large positive entropy change of ~154 cal K^{-1} (mol of enzyme)$^{-1}$. This observation is in full agreement with the fact that the inactive T state assumes a loose, less ordered conformation deduced from data derived from analytical ultracentrifugation and sulfhydryl titrations (*11*), equilibrium gel titrations (*12*), and small-angle neutron scattering (*13*). Steady state kinetic data also indicate that the R → T transition could be entropy-driven (*3*). The structural R → T transition was found to be accompanied by an increase in the isobaric heat capacity change [$\Delta C_{p,\mathrm{R\rightarrow T}}$ = 2.2 kcal K^{-1} (mol of tetramer)$^{-1}$ (Table 1)]. Very large increases in ΔC_p are generally associated with a reversible unfolding of proteins (*29*, *30*). These increases are attributed mainly to the exposure of hydrophobic groups to the solvent and to a consequent reordering of the neighboring water molecules (*31*, *32*). A significant contribution to the observed $\Delta C_{p,\mathrm{R\rightarrow T}}$ increase can be attributed to the solvation of hydrophobic groups. It seems unlikely that ionization of RMPK groups would contribute to the observed $\Delta C_{p,\mathrm{R\rightarrow T}}$, since fewer than one proton was found to be absorbed during the R → T transition and the ΔC_p of protein group ionization was reported to be approximately ±50 cal K^{-1} mol^{-1} (*33*). At 23 °C, the resulting free energy change for the R → T transition can be estimated to be ~3.4 kcal/mol of tetramer, decreasing to zero at 38 °C, which is close to the rabbit body temperature (*34*−*36*). The significance of this finding is discussed in the following paper (DOI: 10.1021/bi900281s).

(*ii*) *Phe Binding*. Results from Table 1 indicate that Phe binding to either the T state or the R state of RMPK is entropically favored with an enthalpy change close to zero. This is a typical situation for an association governed mainly by a change in the solvation state resulting from a release of bound water from the protein or from the ligand. In this case, it is most likely induced mainly by hydrophobic interactions that become stronger at higher temperatures (*37*). Because of the very small values of $\Delta H^{\mathrm{R}}_{\mathrm{Phe}}$ and $\Delta H^{\mathrm{T}}_{\mathrm{Phe}}$, the Phe binding exhibits only very weak temperature dependence.

(*iii*) *PEP Binding*. Binding of PEP to the R state was found to be both entropy- and enthalpy-driven with $\Delta S^{\mathrm{R}}_{\mathrm{PEP}}$ and $\Delta H^{\mathrm{R}}_{\mathrm{PEP}}$ values of 11.2 cal mol^{-1} K^{-1} and −2.1 kcal/mol, respectively. Although electrostatic interactions are expected to dominate, hydrogen bonds can also stabilize the RMPK−PEP complex. Since each hydrogen bond is expected to contribute ~2 kcal/mol to the enthalpy term (*37*), the speculation is that one hydrogen bond could be involved in formation of the complex. Because of the very weak binding of PEP to the T state, the parameters characterizing this interaction could not be accessed from the data with reasonable accuracy. In an attempt to fit enthalpy and entropy terms for the binding of PEP to the T state, no well-defined minimum of the global χ^2 for those parameters was found. The program converged with difficulty, returning diverging nonphysiological $K^{\mathrm{T}}_{\mathrm{PEP}}$ values. When the χ^2 profile was sampled by fixing the $K^{\mathrm{T}}_{\mathrm{PEP}}$ to different values, the χ^2 decreased with an increase in $K^{\mathrm{T}}_{\mathrm{PEP}}$, finally becoming insensitive to any further increase in $K^{\mathrm{T}}_{\mathrm{PEP}}$. The quality of fit was essentially the same whether $K^{\mathrm{T}}_{\mathrm{PEP}}$ was a fitting parameter or fixed to a value

[1]Fit of the ITC data resulting from this global fitting is shown in the preceding paper (DOI: 10.1021/bi900279x).

simulating no binding at all. Consistent with the literature, this result indicates that the affinity of PEP for the T state is much weaker than that for the R state (*3*).

(*iv*) *ADP Binding*. Table 1 shows that the binding of ADP to both the R and T state is enthalpy-driven. The favorable enthalpy decrease is compromised by a relatively large entropy loss. The theoretical limit of a decrease of ~35 cal mol^{-1} K^{-1} in entropy is normally attributed to a full restriction in motional freedom of a ligand in the complex (*37*). Large negative entropy terms found for ADP binding suggest that the contacts between bound ADP and the enzyme significantly restrict the motion of the side chains in the RMPK−ADP complex. Because of the difference in ΔH^{R}_{ADP} and ΔH^{T}_{ADP} values, the ADP dissociation constants exhibit different temperature dependence (eq 5). As a consequence, the differential affinity of ADP for the R and T state varies with temperature. From values given in Table 1, this differential activity can be calculated to be zero near 12 °C where the presence of ADP does not induce shifts in the R ↔ T equilibrium. At higher temperatures, ADP binds more strongly to the R state, causing activation of the enzyme by shifting the R ↔ T equilibrium toward the active R state. Below 12 °C, an inactivating effect of ADP is to be expected.

Coupling between ADP and Phe Binding. The presence of ADP leads to a decrease in the binding enthalpy and entropy for Phe ($\Delta\Delta H^{T}_{ADP,Phe} = -0.54$ kcal mol^{-1} and $\Delta\Delta S^{T}_{ADP,Phe} = -4.9$ cal mol^{-1} K^{-1}, respectively). The decrease indicates that the "ordering effect" induced by ADP is sensed by Phe. Interestingly, in the presence of ADP, the small positive enthalpy term (ΔH^{T}_{Phe}) is diminished [$\Delta H^{T}_{ADP,Phe} = \Delta H^{T}_{Phe} + \Delta\Delta H^{T}_{ADP,Phe} = 0.65 - 0.54$ kcal/mol = 0.11 kcal/mol], rendering the binding of Phe to the T state essentially temperature-independent. At room temperature, the interaction free energy of Phe and ADP ($\Delta\Delta G^{T}_{0}$) can be calculated to be $-540 + 300 \times 4.9 = 0.9$ kcal/mol. This result implies that binding of these ligands in the presence of each other is unfavorable. The value is comparable with the antagonistic interaction energy between Phe and PEP of 1.2 kcal/mol that was previously found with steady state kinetic data (*11*).

DISCUSSION

For the four linked reactions that characterize PK function, at least 21 thermodynamic parameters are required to adequately define the network of linked interactions involved in regulating the allosteric behavior of RMPK. The only chance to define these parameters with accuracy is to overdetermine these parameters with multiple sets of data acquired by different approaches. The ITC data are most useful; however, to garner more data points to enhance the chance of accurately defining these parameters, we employed an additional technique which provides structural information that is sensitive to both ligand binding and conformational changes. A comparison of the results summarized in Table 1 in the preceding paper (DOI: 10.1021/bi900279x) and this work shows clearly the power of multiple approaches and global fitting.

To validate and extend the model established in the preceding paper (DOI: 10.1021/bi900279x), we challenged some of its assumptions. Similar to the calorimetry data, we attempted to fit the IFT data with $\Delta C_{p,R\rightarrow T}$ fixed to zero. Under these conditions, the fitting program never converged. This indicates inconsistency of $\Delta C_{p,R\rightarrow T} = 0$ not only with the ITC data but also with the fluorescence data. After $\Delta C_{p,R\rightarrow T}$ was allowed to be a parameter to be defined, the fitting converged to the values presented in Table 1.

We also verified the coupling between the interactions involving Phe and ADP reported in the preceding paper (DOI: 10.1021/bi900279x). An analysis of the full data set without accounting for the ADP−Phe interaction (the $\Delta\Delta H^{T}_{ADP,Phe}$ and the $\Delta\Delta S^{T}_{ADP,Phe}$ terms were fixed to zero) led to fits with unacceptable statistics. This confirms the presence of an antagonistic coupling between ADP and Phe binding.

In addition to the thermodynamic parameters, nine spectroscopic parameters were derived from the fluorescence data, providing structural characterizations of the R and T states. To further challenge the fitted model from the viewpoint of structural information, fluorescence parameters from Table 1 were used to simulate the dependence of the $^{sat}I_{ADP}/I_0$ ratio on temperature. The result calculated according to eq 10 is shown in Figure 5 by the solid line. At temperatures between 30 and 45 °C, the simulation predicts a decrease in the $^{sat}I_{ADP}/I_0$ ratio that results from the activation of RMPK which is present in a higher population of the less fluorescent R state due to the higher binding affinity of ADP for the R state. Figure 5 shows that the simulation is in good qualitative and quantitative agreement with the measured data. Because the experimental data from Figure 5 were not used for the fitting, the agreement between the prediction and the experimental data is a fully independent test of the validity of the model. It is most interesting to note that the ratio of fluorescence intensity reaches a minimum at ~40 °C, indicating that the optimal temperature for 10 mM ADP to switch RMPK to the active R state is 40 °C. However, at higher temperatures, the trend is reversed. This indicates that the state distribution of RMPK is reversed in favor of the T state. This reversal of behavior is the direct consequence of the favoring of the R ↔ T equilibrium toward the T state at these higher temperatures.

The FTS data in Figure 6 show the shift in the state of RMPK by temperature in the presence of various combinations of ADP and Phe concentrations. At 12 mM Phe, RMPK is in the T state which is characterized by a high quantum yield. A decrease in the ratio of fluorescence intensity indicates a decrease in the fraction of the T state and an increase in the fraction of the R state which exhibits a low quantum yield. The FTS data shown in Figure 6A indicate that at a low ADP concentration of 1 mM and 12 mM Phe there was no state change in RMPK induced by temperature. This is due to the fact that there was not enough ADP to bind to RMPK to affect the distribution of states in RMPK. At 2 mM ADP and 12 mM Phe, there was a slight decrease in the fluorescence intensity ratio at low temperatures, implying a shift toward the R state under those conditions. At 10 mM ADP and 12 mM Phe, there was a significant drop in the ratio at low temperatures. The ratio approaches 1.0 at higher temperatures. This behavior is a reflection of the effect of temperature on the R ↔ T equilibrium and the reversal of the ratio of affinity of ADP for the R and T states (see ADP Binding in Results). To test the validity of the derived parameters in Table 1, we simulated the temperature dependence of the $^{sat}I_{ADP,Phe}/^{sat}I_{Phe}$ ratio in the presence of 12 mM Phe and 10 mM ADP as depicted in Figure 6B. The curve was calculated using eq 10 twice and making the ratio $^{sat}I_{ADP,Phe}/^{sat}I_{Phe}$ equal to $(^{sat}I_{ADP,Phe}/I_0)/(^{sat}I_{Phe}/I_0)$. It is obvious that the predicted dependence is in good qualitative agreement with the experimental data shown in Figure 6A. When the simulation was performed by neglecting the ADP−Phe coupling, the simulated $^{sat}I_{ADP,Phe}/^{sat}I_{Phe}$ ratio was unity at all temperatures. This did not agree with the measured data. Since the FTS data from Figure 6A were not included in the global fitting, the observed agreement between the

predicted and measured effects strongly supports both the validity of the fitted model and the conclusions about the role of ADP in the allosteric regulation of RMPK.

Upon closer examination, there is an apparent discrepancy between data shown in Figures 5 and 6. While in Figure 5 the activating effect of ADP is most pronounced at high temperatures and almost no effect is seen below 30 °C, in Figure 6 the opposite was observed. In the presence of Phe, activation of RMPK was observed at low temperatures and the effect decreased with an increase in temperature. The clue is in the high-temperature dependence of the equilibrium constant L_0 describing the R ↔ T equilibrium. Using the parameters in Table 1, it can be shown that more than 96% of RMPK is in the active state at 30 °C or lower temperatures and the activating effect of ADP is therefore insignificant, as shown in Figure 5. At 45 °C, the R → T transition is almost complete and the activation by ADP does not dominate over this R → T transition. The combined effect of temperature and Phe inhibition leads to no observable effect of ADP in the presence of Phe above 30 °C (Figure 6).

In conclusion, complementation of the fluorescence experiments with the ITC data (DOI: 10.1021/bi900279x) allowed for characterization of multiple linked equilibria associated with an allosteric regulation of the RMPK. Global data analysis played an essential role in this process since we could quantify parameters that would not be easily accessible by other means. Importantly, we confirmed an increase in the isobaric heat capacity associated with the entropy-driven R → T transition and an intriguing role of ADP in the enzyme activation process. A graphical representation of current results, their physiological relevance, and simulated predictions of the RMPK allosteric regulation is presented in the following paper (DOI: 10.1021/bi900281s).

Remarks on Global Fitting. Nonlinear least-squares data analysis is often used for validation of a theoretical model that describes data under investigation since it looks for an objective comparison between the experimental data and the proposed model (*18*). As the model becomes complicated and the number of model parameters increases, the fitting problem starts to be ill-defined because data do not carry enough information for the accurate recovery of all parameters. In other words, the minimum of the χ^2 surface starts to be too shallow and correlation between parameters becomes too high to determine correct parameter values with confidence. A very powerful approach that helps to sharpen the χ^2 minimum and to remove the correlation between parameters is a simultaneous analysis of multiple data sets acquired under different experimental conditions and/or with different techniques, the global analysis (*16*, *20*). The global analysis is an extension of a conventional least-squares fitting for simultaneous analysis of multiple data sets under a single model that encompasses them all. An important feature of this approach is that model parameters may be common for different curves. Such parameter linkage overdetermines the model and sharpens the χ^2 surface (*16*). The global analysis has been previously used for a large variety of different experimental data and experimental techniques (DOI: 10.1021/bi900279x) (*1*, *17*, *21*−*25*, *38*, *39*). In all cases, it provided performance far beyond the resolution of the conventional analysis.

Our model needs 30 parameters to describe allosteric regulation of RMPK in the presence of the three examined ligands (Table 1). This number is definitely too high to recover them all from a single experiment. Fortunately, under carefully chosen experimental conditions, e.g., in the presence of single ligands, the number of parameters analytically describing the individual curves significantly decreases. It is not unusual in the literature to analyze a single experimental curve containing a dozen points with a three- to five-parameter model. In this study, 27 independent curves with more than 1600 experimental points were globally analyzed. From this point of view, the current statistics of ~1.1 parameter per curve and 55 data points per parameter are rather favorable and allow for good model validation. Moreover, many parameters are common for multiple data sets. For instance, parameters $S_{0,R\rightarrow T}$, $H_{0,R\rightarrow T}$, and $\Delta C_{p,R\rightarrow T}$ characterizing the R → T equilibrium are common for 26 of 27 curves, and due to strong overdetermination, they were recovered with good accuracy.

During the data analysis, we became aware that the multidimensional χ^2 surface contains local minima. To avoid being trapped in such minima, the fitting was initiated with the limited data set (and limited number of parameters) from isothermal calorimetry. The known parameters were fixed, and fluorescence curves were added individually or in groups with subsequent fitting. After optimization, all parameters were released and the system was optimized again. This procedure was repeated for several different sequences with expansion of the global data set. This procedure always resulted in the same final set of parameter values. The global fitting with numerous sets of initial parameter guesses was performed to make sure that the fitting converges to the same global minimum.

ACKNOWLEDGMENT

We thank Drs. X. Cheng and A. Gribenko for critical review of the manuscript. This series of papers is dedicated to Professor Serge N. Timasheff who taught us the beauty and power of thermodynamics of linked reactions in biology.

REFERENCES

1. Oberfelder, R. W., Barisas, B. G., and Lee, J. C. (1984) Thermodynamic linkages in rabbit muscle pyruvate kinase: Analysis of experimental data by a two-state model. *Biochemistry 23*, 3822–3826.
2. Consler, T. G., Jennewein, M. J., Cai, G. Z., and Lee, J. C. (1990) Synergistic effects of proton and phenylalanine on the regulation of muscle pyruvate kinase. *Biochemistry 29*, 10765–10771.
3. Consler, T. G., Jennewein, M. J., Cai, G. Z., and Lee, J. C. (1992) Energetics of Allosteric Regulation in Muscle Pyruvate Kinase. *Biochemistry 31*, 7870–7878.
4. Consler, T. G., Woodard, S. H., and Lee, J. C. (1989) Effects of primary sequence differences on the global structure and function of an enzyme: A study of pyruvate kinase isozymes. *Biochemistry 28*, 8756–8764.
5. Jones, B. E., Beechem, J. M., and Matthews, C. R. (1995) Local and global dynamics during the folding of *Escherichia coli* dihydrofolate reductase by time-resolved fluorescence spectroscopy. *Biochemistry 34*, 1867–1877.
6. Tang, K. E., and Dill, K. A. (1998) Native protein fluctuations: The conformational-motion temperature and the inverse correlation of protein flexibility with protein stability. *J. Biomol. Struct. Dyn. 16*, 397–411.
7. Tilton, R. F. Jr., Dewan, J. C., and Petsko, G. A. (1992) Effects of temperature on protein structure and dynamics: X-ray crystallographic studies of the protein ribonuclease-A at nine different temperatures from 98 to 320 K. *Biochemistry 31*, 2469–2481.
8. Lakowicz, J. R. (1999) Principles of fluorescence spectroscopy, 2nd ed., Kluwer Academic/Plenum Publishers, New York.
9. Yu, H. T., Vela, M. A., Fronczek, F. R., McLaughlin, M. L., and Barkley, M. D. (1995) Microenvironmental Effects on the Solvent Quenching Rate in Constrained Tryptophan Derivatives. *J. Am. Chem. Soc. 117*, 348–357.

10. Wooll, J. O., Friesen, R. H., White, M. A., Watowich, S. J., Fox, R. O., Lee, J. C., and Czerwinski, E. W. (2001) Structural and functional linkages between subunit interfaces in mammalian pyruvate kinase. *J. Mol. Biol. 312*, 525–540.
11. Oberfelder, R. W., Lee, L. L., and Lee, J. C. (1984) Thermodynamic linkages in rabbit muscle pyruvate kinase: Kinetic, equilibrium, and structural studies. *Biochemistry 23*, 3813–3821.
12. Heyduk, E., Heyduk, T., and Lee, J. C. (1992) Global conformational changes in allosteric proteins. A study of *Escherichia coli* cAMP receptor protein and muscle pyruvate kinase. *J. Biol. Chem. 267*, 3200–3204.
13. Consler, T. G., Uberbacher, E. C., Bunick, G. J., Liebman, M. N., and Lee, J. C. (1988) Domain interaction in rabbit muscle pyruvate kinase. II. Small angle neutron scattering and computer simulation. *J. Biol. Chem. 263*, 2794–2801.
14. Yu, S., Lee, L. L., and Lee, J. C. (2003) Effects of metabolites on the structural dynamics of rabbit muscle pyruvate kinase. *Biophys. Chem. 103*, 1–11.
15. Larsen, T. M., Laughlin, L. T., Holden, H. M., Rayment, I., and Reed, G. H. (1994) Structure of rabbit muscle pyruvate kinase complexed with Mn^{2+}, K^{+}, and pyruvate. *Biochemistry 33*, 6301–6309.
16. Knutson, J. R., Beechem, J. M., and Brand, L. (1983) Simultaneous Analysis of Multiple Fluorescence Decay Curves: A Global Approach. *Chem. Phys. Lett. 102*, 501–507.
17. Beechem, J. M., Knutson, J. R., Ross, J. B. A., Turner, B. W., and Brand, L. (1983) Global Resolution of Heterogeneous Decay by Phase Modulation Fluorometry: Mixtures and Proteins. *Biochemistry 22*, 6054–6058.
18. Bevington, P. R., and Robinson, D. K. (2002) Data reduction and error analysis for the physical sciences , 3rd ed., McGraw-Hill, New York.
19. Marquardt, D. W. (1963) An Algorithm for Least-Squares Estimation of Nonlinear Parameters. *J. Soc. Ind. Appl. Math. 11*, 431–441.
20. Beechem, J. M., Ameloot, M., and Brand, L. (1985) Global and target analysis of complex decay phenomena. *Anal. Instrum. 14*, 379–402.
21. Eisenfeld, J., and Ford, C. C. (1979) A systems-theory approach to the analysis of multiexponential fluorescence decay. *Biophys. J. 26*, 73–83.
22. Boo, B. H., and Kang, D. (2005) Global and target analysis of time-resolved fluorescence spectra of di-9H-fluoren-9-yldimethylsilane: Dynamics and energetics for intramolecular excimer formation. *J. Phys. Chem. A 109*, 4280–4284.
23. Ionescu, R. M., and Eftink, M. R. (1997) Global analysis of the acid-induced and urea-induced unfolding of staphylococcal nuclease and two of its variants. *Biochemistry 36*, 1129–1140.
24. Ucci, J. W., and Cole, J. L. (2004) Global analysis of non-specific protein-nucleic interactions by sedimentation equilibrium. *Biophys. Chem. 108*, 127–140.
25. Verveer, P. J., Squire, A., and Bastiaens, P. I. (2000) Global analysis of fluorescence lifetime imaging microscopy data. *Biophys. J. 78*, 2127–2137.
26. Vermunicht, G., Boens, N., and de Schryver, F. C. (1991) Global analysis of the time-resolved fluorescence of α-chymotrypsinogen A and α-chymotrypsin powders as a function of hydration. *Photochem. Photobiol. 53*, 57–63.
27. Monod, J., Wyman, J., and Changeux, J. P. (1965) On the Nature of Allosteric Transitions: A Plausible Model. *J. Mol. Biol. 12*, 88–118.
28. Cantor, C. R., and Schimmel, P. R. (1980) Biophysical chemistry, part 3, W. H. Freeman & Co., San Francisco.
29. Jackson, W. M., and Brandts, J. F. (1970) Thermodynamics of protein denaturation. A calorimetric study of the reversible denaturation of chymotrypsinogen and conclusions regarding the accuracy of the two-state approximation. *Biochemistry 9*, 2294–2301.
30. Privalov, P. L., Khechinashvili, N. N., and Atanasov, B. P. (1971) Thermodynamic analysis of thermal transitions in globular proteins. I. Calorimetric study of chymotrypsinogen, ribonuclease and myoglobin. *Biopolymers 10*, 1865–1890.
31. Kauzmann, W. (1959) Some factors in the interpretation of protein denaturation. *Adv. Protein Chem. 14*, 1–63.
32. Tanford, C. (1970) Protein denaturation. C. Theoretical models for the mechanism of denaturation. *Adv. Protein Chem. 24*, 1–95.
33. Edsall, J. T., and Wyman, J. (1958) Biophysical Chemistry , Vol. I, Academic Press, New York.
34. Sutherland, G. B., Trapani, I. L., and Campbell, D. H. (1958) Cold adapted animals. II. Changes in the circulating plasma proteins and formed elements of rabbit blood under various degrees of cold stress. *J. Appl. Physiol. 12*, 367–372.
35. Gonzalez, R. R., Kluger, M. J., and Hardy, J. D. (1971) Partitional calorimetry of the New Zealand white rabbit at temperatures 5−35 °C. *J. Appl. Physiol. 31*, 728–734.
36. McEwen, G. N. Jr., and Heath, J. E. (1973) Resting metabolism and thermoregulation in the unrestrained rabbit. *J. Appl. Physiol. 35*, 884–886.
37. Eftink, M. R., and Biltonen, R. L. (1980) in Biological microcalorimetry (Breezer, A. E., Ed.) pp 343−412, Academic Press, New York.
38. Barisas, B. G., and Gill, S. J. (1979) Thermodynamic analysis of carbon monoxide binding by hemoglobin trout I. *Biophys. Chem. 9*, 235–244.
39. Gilbert, C. W. (1980) A vector method for non-linear least squares reconvolution and fitting analysis of polarized fluorescence decay data. In Time-resolved fluorescence spectroscopy in biochemistry and biology (Nato ASI Series) (Dale, R. E., and Cundall, R. B., Eds.) Plenum Press, New York.
40. Christensen, J. J., Hansen, L. D., and Reed, M. I. (1976) Handbook of Proton Ionization Heats and Related Thermodynamic Quantities , John Wiley & Sons, New York.
41. Eftink, M. R., Selvidge, L. A., Callis, P. R., and Rehms, A. A. (1990) Photophysics of indole-derivatives: Experimental resolution of La and Lb transitions and comparison with theory. *J. Phys. Chem. 94*, 3469–3479.
42. Obsilova, V., Herman, P., Vecer, J., Sulc, M., Teisinger, J., and Obsil, T. (2004) 14-3-3ζ C-terminal stretch changes its conformation upon ligand binding and phosphorylation at Thr232. *J. Biol. Chem. 279*, 4531–4540.